MCB
Journals.ASM.org

Acyl Coenzyme A Thioesterase 7 Regulates Neuronal Fatty Acid Metabolism To Prevent Neurotoxicity

Jessica M. Ellis,[a] G. William Wong,[b] Michael J. Wolfgang[a]

Departments of Biological Chemistry[a] and Physiology,[b] Johns Hopkins University School of Medicine, Center for Metabolism and Obesity Research, Baltimore, Maryland, USA

Numerous neurological diseases are associated with dysregulated lipid metabolism; however, the basic metabolic control of fatty acid metabolism in neurons remains enigmatic. Here we have shown that neurons have abundant expression and activity of the long-chain cytoplasmic acyl coenzyme A (acyl-CoA) thioesterase 7 (ACOT7) to regulate lipid retention and metabolism. Unbiased and targeted metabolomic analysis of fasted mice with a conditional knockout of ACOT7 in the nervous system, *Acot7*$^{N-/-}$, revealed increased fatty acid flux into multiple long-chain acyl-CoA-dependent pathways. The alterations in brain fatty acid metabolism were concomitant with a loss of lean mass, hypermetabolism, hepatic steatosis, dyslipidemia, and behavioral hyperexcitability in *Acot7*$^{N-/-}$ mice. These failures in adaptive energy metabolism are common in neurodegenerative diseases. In agreement, *Acot7*$^{N-/-}$ mice exhibit neurological dysfunction and neurodegeneration. These data show that ACOT7 counterregulates fatty acid metabolism in neurons and protects against neurotoxicity.

Neurons have a unique lipid composition that is critical for the development and function of the nervous system, and defects in lipid metabolism result in severe and debilitating neurological disease; however, there is a dearth of understanding about how neurons uniquely regulate intracellular fatty acid (FA) metabolism. There are numerous inborn errors of lipid metabolism that have clear neuropathological outcomes. Apart from these inborn errors of metabolism, it is becoming increasingly evident that many neurodegenerative diseases, including Alzheimer's disease, Parkinson's disease, and amyotrophic lateral sclerosis (ALS), have underlying metabolic dysfunction that often involves dysregulated lipid metabolism (1–5). A better understanding of neuronal metabolism is required to provide insight into neurological function and pathology, since dysregulated neurometabolism may contribute to the progression of diabetes and obesity and hasten neurodegeneration (6–8).

Fatty acid metabolism in the nervous system has been shown to directly and profoundly regulate multiple aspects of animal physiology and behavior (9–14). Furthermore, ion channels that play a role in neuronal activation have been shown to be regulated by lipids either directly or indirectly (15–20). Fatty acids are precursors for membrane biosynthesis, signaling lipids, posttranslational modification (e.g., palmitoylation), energy storage, and energy production. Although most neurons are not thought to rely on fatty acids to meet their cellular bioenergetic requirements, the brain has a unique fatty acid composition and metabolism that are critical for neural function. Due in part to the incredible heterogeneity of neurons themselves and the diversity of neuronal cell types in general, the means by which any neuronal population obtains or utilizes fatty acids is poorly understood.

Fatty acids either made *de novo* or taken up from the diet require ligation to coenzyme A (CoA) for their cellular retention and activation by one of 26 known acyl-CoA synthetases (21). The resulting acyl-CoAs, with their high-energy thioester linkage, are used as the substrate for almost all anabolic and catabolic biochemical reactions requiring fatty acids, with the noted exception of eicosanoid synthesis. The hydrolysis of acyl-CoAs to free fatty acid (FFA) and free CoA by one of a family of acyl-CoA thioesterases has been proposed to play a regulatory role in the metabolism of fatty acids (22–25). Acyl-CoA thioesterases (ACOTs) are present in simple prokaryotes and conserved and expanded through humans. Mammals express acyl-CoA thioesterases that have various chain length specificities, cell type expression, and subcellular localizations (22). Although some of the basic enzymatic characteristics of ACOTs have been previously reported, little is known about the biochemical or physiologic significance of this enigmatic class of enzymes in a cellular or organismal context. Neurons have a particularly high cytoplasmic long-chain acyl-CoA hydrolase activity, which is thought to be mediated mainly by Acyl-CoA thioesterase 7 (ACOT7) (26). The high activity and cytoplasmic localization of an acyl-CoA hydrolase such as ACOT7 creates an apparently futile cycle because it is juxtaposed to the ATP-dependent Acyl-CoA synthetases. Given its biochemical activity, localization, and chain length specificity, ACOT7 likely represents a major regulatory point in neural fatty acid metabolism by limiting the access of long-chain acyl-CoAs. Acyl-CoA hydrolysis provides neurons with a unique means to regulate fatty acid metabolism because neurons have a limited capacity for neutral lipid storage and mitochondrial fatty acid beta oxidation.

Here we have shown that ACOT7 is highly expressed in neurons and constitutes the main source of acyl-CoA thioesterase activity in the brain. Using a conditional knockout (KO) of ACOT7 in the nervous system, we have shown that ACOT7 regulates the metabolism of long-chain fatty acids into multiple acyl-CoA-dependent pathways. The biochemical consequences of a

Received 14 November 2012 **Returned for modification** 7 December 2012
Accepted 21 February 2013
Published ahead of print 4 March 2013
Address correspondence to Michael J. Wolfgang, mwolfga1@jhmi.edu.
Supplemental material for this article may be found at http://dx.doi.org/10.1128/MCB.01548-12

doi:10.1128/MCB.01548-12

loss of ACOT7 are largely not apparent in fed mice and are greatly exacerbated by fasting, a time when circulating free fatty acids from lipolysis are elevated. ACOT7 brain-specific KO mice have no alterations in food intake or body weight; however, KO mice have multiple alterations in behavior and physiology, including a loss of lean mass, hypermetabolism, hepatic steatosis, dyslipidemia, and behavioral hyperexcitability. These phenotypic changes are seen in models of neurodegeneration, and ACOT7 KO mice exhibit neurodegeneration and neurological/behavioral deficits. These data suggest that ACOT7 is required to maintain neuronal fatty acid homeostasis, particularly during fasting, and dysregulation of ACOT7 results in neural lipotoxicity.

MATERIALS AND METHODS

Mice. Acot7$^{flox/flox}$ mice were generated by targeting loxP sequences to introns flanking exon 2 of the mouse *acot7* gene by homologous recombination in C57BL/6 embryonic stem cells by standard methods. *Acot7*$^{N-/-}$ and littermate *Acot7*$^{flox/flox}$ control mice were housed (12-h light/dark cycle) with free access to water and a chow diet (13.5% kcal from fat; number 5001, LabDiet; PMI Nutrition International, St. Louis, MO) or a high-fat diet (HFD) (60% kcal from fat, D12492; Research Diets). Body fat mass was assessed by magnetic resonance imaging analysis (QNMR EchoMRI100; Echo Medical Systems, LLC). For thermogenesis experiments, mice were fasted overnight or fed *ad libitum* and placed in a 4°C environment without food. Temperature was measured hourly with a rectal probe thermometer (BAT-12; Physitemp).

Calorimetry and behavior. Locomotor activity, food intake, and whole-body calorimetry were determined in an open-circuit indirect calorimeter (Oxymax Equal Flow; Columbus Instruments). Data were collected after a 24-h acclimation period. Rates of oxygen consumption (VO_2, ml/kg/h) and carbon dioxide production (VCO_2) were measured for each chamber every 15 min throughout the study. The respiratory exchange ratio (RER) (VCO_2/VO_2) was calculated by using Oxymax software (v. 4.02) to estimate the relative oxidation of carbohydrate (RER = 1.0) versus fat (RER approaching 0.7), not accounting for protein oxidation. Heat (energy expenditure) was calculated as follows: heat = $VO_2 \times [3.815 + (1.232 \times \text{RER})]$; this was normalized for subject lean mass (kcal/kg lean mass/h). Ambulatory activity was measured by the counts of beam breaks monitored across a single plane using the infrared (IR) photocell technology built into the CLAMS (comprehensive lab animal monitoring system) chambers.

Motor coordination on a rotarod treadmill (no. Env-575m; Med Associate Inc.) was assessed by a blinded investigator. Mice were rotarod trained with three tests on 2 different days, 1 day apart; experimental data were obtained using the Rota-Rod software program and calculated based on the average time spent on the rod over three tests as the rod rotation accelerated from 4 rpm to 40 rpm over 500 s.

Ataxia was screened by a blinded investigator for four phenotypic measures, hind limb clasping, ledge test, gait, and kyphosis. Ataxia test values were calculated by the average for three trials, in which mouse performance was scored between 0 to 3 for best to worst performance as previously described (27). Open field tests were performed by placing the mouse in the center of the open field apparatus, and beam breaks were monitored over a 40-min time period; data are presented as the sum of movement over the 40-min period for 3- to 5-month-old male mice.

Acoustic startle response/prepulse inhibition was measured in startle chambers (San Diego Instruments, Inc., San Diego, CA). Acoustic stimuli were controlled by the SR-LAB software program (San Diego Instruments, Inc., San Diego, CA) and interface system, which rectifies, digitizes, and records responses from the accelerometer. The maximum voltages within 100-ms reading windows, starting at stimulus onset, were used as measures of startle amplitudes. Sound levels were measured inside the startle cabinets by means of the digital sound level meter (Realistic; Tandy, Fort Worth, TX, USA). The experimental session consists of a 5-min acclimatization period to a 70-dB background noise (continuous throughout the session), followed by the presentation of 10 40-ms 120-dB white-noise stimuli at a 20-s interstimulus interval (the habituation session). Upon completion of the habituation session, each mouse was left in the enclosure for 5 min without presentation of any startle stimuli. Immediately after, the prepulse inhibition (PPI) session was begun. During each PPI session, a mouse was exposed to the following types of trials: pulse-alone trial (a 120-dB, 100-ms, broadband burst), the omission of stimuli (no-stimulus trial), and five prepulse-pulse combinations (prepulse-pulse trials) consisting of a 20-ms broadband burst used as a prepulse and presented 80-ms before the pulse using one of the five prepulse intensities: 74, 78, 82, 86, and 90 dB. Each session consists of six presentations of each type of trial presented in a pseudorandom order. PPI is assessed as the percentage scores of PPI (%PPI): [1 − (average startle amplitude after prepulse/average startle amplitude after pulse only)] × 100 for each animal separately.

All procedures were performed in accordance with the National Institutes of Health Guide for the Care and Use of Laboratory Animals and under the approval of the Johns Hopkins Medical School Animal Care and Use Committee.

Metabolite analysis. Plasma triacylglycerol (TAG) (Sigma), β-hydroxybutyrate (Stanbio), cholesterol (BioAssay Systems), FFA (Wako), glucose (GlucometerX; BioAssay Systems), creatine kinase (Cayman), and free and total glycerol (Sigma) were measured colorimetrically. Brain coenzyme A content was measured fluorometrically (Cayman Chemicals). Acyl-CoAs were measured by high-performance liquid chromatography (HPLC) as detailed elsewhere (28). Unbiased metabolomics analysis was done as described previously (29). Brain and liver total lipids were extracted with chloroform-methanol via the Folch method (30), the chloroform phase was dried down by using a Centrivac concentrator (Labconco) and resuspended in *tert*-butanol–methanol–Triton X-100 (3:1:1 ratio, by volume), and lipids were quantified using the colormetric assay described above and by use of a PL kit (BioAssay Systems). Total acyl-CoA thioesterase was measured using 50 μM oleoyl-CoA (Sigma) and 10 mM 5,5′-dithiobis(2-nitrobenzoate) (DTNB) (Sigma) with CoA standards run in parallel in either total homogenate or cytosol fractions (2.5 to 25 μg). Cytosolic phospholipase A_2 was measured with 50 mM Tris-HCl, 5 mM EDTA, 0.1% bovine serum albumin (BSA), 2 μM β-1-hexadecanoyl-2-(1-pyrenedecanoyl)-*sn*-glycero-3-phosphocholine (β-Py-C10-HPC) (Invitrogen), 6 mM $CaCl_2$, and 100 mM NaCl in cytosolic fractions isolated from mouse brains. Release of 1-pyrenedecanoyl from β-Py-C10-HPC was read fluorometrically with excitation at 345 nm and emission at 377 nm after 20 min at room temperature. Acyl-CoA synthetase activity was measured in brain total particulate as previously described (31).

Gene expression. Acot7 mRNA abundance across tissues was determined per the manufacturer's instruction (Origene). Tissue RNA was isolated using Qiagen RNeasy kits, cDNA was synthesized (High Capacity cDNA reverse transcription [RT] kit; Applied Biosystems), and the reaction was carried out using SYBR green (Bio-Rad) detection with specific primers (200 nM) and equal amounts of cDNA (10 ng/reaction) and analyzed by using a CFX Connect thermocycler (Bio-Rad). Results were normalized to the housekeeping gene and expressed as arbitrary units of $2^{\times\Delta\Delta CT}$.

Immunoblots and histology. Total homogenates were collected in sucrose medium (10 mM Tris, 1 mM EDTA, and 250 mM sucrose). Lysates were collected in lysis buffer (50 mM Tris-HCl, 150 mM NaCl, 1 mM EDTA, 1% Triton X-100). Cytosol and membrane fractions collected from total homogenates in sucrose medium were separated by centrifuged at 40,000 × *g* for 1 h. Homogenates, lysates, cytosol, or membrane fractions were equally loaded (20 to 50 μg) and electrophoresed on 8% or 12% SDS polyacrylamide gels, transferred to a polyvinylidene difluoride (PVDF) membrane, blocked with 5% milk-TBST (Tris-buffered saline with Tween 20) for 1 h, incubated with primary antibody (1:1,000 to 1:2,000) against ACOT7 (affinity purified against the peptide EKKRFEEGKGRYLQMK), MitoProfile Total Oxphos rodent Western

blot (WB) antibody cocktail (ab110413; AbCam), glial fibrillary acidic protein (GFAP) (Chemicon), dismutase 2 (SOD2; Abcam), voltage-dependent anion channel 1 (VDAC1) (Calbiochem), cytochrome *c* oxidase (CoxIV; BD Biosciences), and HSC70 (Santa Cruz), washed, and incubated with secondary antibody conjugated to horseradish peroxidase (HRP) (GE Healthcare), Cy3, or Cy5 (1:2,000) (Invitrogen). Protein was visualized using an Alpha Innotech MultiImage III instrument and quantified using Alpha Innotech FluorChem Q software (Santa Clara, CA). For histology, half of brains, cut sagitally, were fixed in 4% paraformaldehyde–phosphate-buffered saline (PBS) for 4 h, washed with PBS (3×), transferred to 9% sucrose-PBS overnight, and then transferred to 30% sucrose overnight, and tissue was frozen in OCT compound. Sagittal sections were cut 18 μm thick using a cryostat. For Nissl staining, cleared and rehydrated sections were incubated with 0.5% cresyl violet acetate, washed, rapidly dehydrated, cleared, and mounted on coverslips. Images were taken at magnification ×4, and the width of the granular cell layer relative to the lobule width was measured using the Image J software program in an investigator-blinded manner; at least 10 measurements were taken per mouse and averaged together, and data are presented as the average for 6 to 8 mice per group. For liver histology, tissue was fixed in 4% paraformaldehyde-PBS for 24 h, transferred to 70% ethanol, embedded in paraffin, serially sectioned, and stained with hematoxylin and eosin (H&E) (AML Laboratories Inc.). For transmission electron microscopy (TEM), mice were perfused with a 2% paraformaldehyde, 2% glutaraldehyde-PBS solution, and a 3-mm^3 block of hippocampus and cortex was excised and further processed for TEM with osmium tetroxide. Ultrathin sections were then cut and imaged using a Hitachi 7600 TEM.

Brain slice studies. Brain slices were collected from overnight-fasted mice, and whole brains were immediately sliced coronally into 350 μM sections using the McIlwain tissue chopper. Slices were incubated in 20% neurobasal medium (Invitrogen), 0.5 mM L-carnitine, 0.2% BSA, and 25 μM glutamine, with either [1-^{14}C]oleate (PerkinElmer), [U-^{14}C]glucose, or [^{3}H]acetate in a 37°C water bath for 1 to 3 h with gentle shaking. Rates of CO_2 and acid-stable metabolite (ASM) production from [1-^{14}C]oleate were determined using incubation chambers containing a center well filled with filter paper and sealed with a rubber stopper. Carbon dioxide was trapped by adding 200 μl 70% perchloric acid to the reaction mixture and 300 μl of 1 M NaOH to the center well and incubating the samples at 55°C for 1 h. The filter paper was then placed in scintillation fluid and counted. The acidified reaction mixture was incubated overnight at 4°C and centrifuged at 4,000 rpm for 30 min before aliquots of the supernatant were counted for ^{14}C-labeled ASM. All slice experiments were performed with 3 to 4 slices per assay per mouse and averaged over 3 independent experiments. FA incorporation was measured by incubating slices with [1-^{14}C]oleate for 16 h, after which slices were washed 3 times with 1% BSA-PBS. Total lipid was extracted from slices that were manually homogenized using a glass mortar and pestle and extracted into $CHCl_3$ (32), mixed with scintillation fluid, and counted.

RESULTS

ACOT7 is highly and selectively expressed in neurons. ACOT7, also known as brain acyl-CoA hydrolase, was previously shown to be enriched in the brain (33–35). We performed Northern blot analysis of various tissues and showed that *acot7* mRNA is expressed at high levels in the brain and testes (Fig. 1A). To characterize Acot7 expression across the brain, we performed RT-PCR for *acot7* on cDNA made from different developmental stages of the mouse brain and across brain regions (see Fig S1A in the supplemental material). These data show persistent and high Acot7 expression across brain development and brain regions. To confirm that mRNA content correlates with protein levels, we produced rabbit polyclonal antibodies against a C-terminal peptide of ACOT7. The specificity of the antibody was confirmed in ACOT7 KO mice (Fig. 2C). Western blot analysis of mouse tissues showed that the testis produced little protein from its abundant mRNA and that the brain has by far the highest expression of the ACOT7 protein (Fig. 1B; see also Fig. S1B). To determine the cell population that ACOT7 is predominately expressed in, we isolated primary cortical neurons and astrocytes and showed by both protein and mRNA that ACOT7 is highly expressed in neurons, not astrocytes, consistent with *in situ* hybridization data (Fig. 1C and D) (36). To determine the subcellular localization of ACOT7 in neurons, we expressed a C-terminal enhanced green fluorescent protein (eGFP) fusion of ACOT7 in primary cortical neurons and showed that ACOT7 is primarily cytoplasmic (Fig. 1E). To further confirm cytoplasmic localization of endogenous ACOT7, we separated mouse brain cytosolic and membrane fractions to probe for ACOT7. Endogenous ACOT7 is expressed predominately in the cytosolic fraction (see Fig. S1C). Finally, we profiled the expression of ACOT7 by Western blotting and measured total long-chain thioesterase activity in multiple regions of the brain and peripheral tissues in fed control, overnight-fasted control, and ACOT7 KO mice (Fig. 1F and G). While neither ACOT7 protein nor thioesterase activity was consistently changed between the fed and fasted state in the various tissues, it is clear that the brain, particularly the hypothalamus, which has the highest access to fatty acids, has higher ACOT7 protein abundance and total thioesterase activity than any other tissue assayed. Together, these data show that ACOT7 is highly and selectively expressed in the cytosol of neurons.

Brain acyl-CoA thioesterase activity is mediated by ACOT7. To understand the biochemical and physiological role of ACOT7 *in vivo*, we generated transgenic mice with a conditional allele of *Acot7*. LoxP sequences were targeted to introns flanking exon 2 of the mouse *acot7* gene by homologous recombination in C57BL/6 embryonic stem cells (Fig. 2A and B). Exon 2 contains an asparagine that is critical for thioesterase function and is conserved in all active ACOT7 variants (37). Excision of exon 2 results in an alternative splicing and premature stop codons in exon 3. Because we are interested in the role of ACOT7 in brain metabolism, we bred $Acot7^{flox/flox}$ mice to Nestin-Cre transgenic mice (12, 38, 39) to produce mice with ACOT7 specifically deleted in the nervous system ($Acot7^{N-/-}$). Knockout of ACOT7 in the brain results in a null allele (Fig. 2C). A small amount of ACOT7 is still present, presumably from expression in nonparenchymal tissue, such as microglia (40). The knockout of ACOT7 in the brain is not lethal; mice are born at the expected Mendelian ratio with no apparent developmental defects, behavioral abnormalities, or structural defects (Fig. 2D). Thioesterase activity is almost completely abolished in the brains of these mice (Fig. 2E), indicating that Acot7 contributes the majority of long-chain thioesterase activity in the brain and that none of the other thioesterases compensated for the loss in ACOT7. The small remaining thioesterase activity is from a combination of ACOT7 expressed in nonneuronal cells and the other thioesterase isoforms that are expressed at minor levels in the brain. There was no compensatory loss of total long-chain acyl-CoA synthetase activity, the reaction that generates acyl-CoA from free fatty acid and CoA (Fig. 2F). The >80% loss of total thioesterase activity suggests a potential increase in acyl-CoA content in the brain; however, the steady-state concentration of long-chain acyl-CoAs did not change (Fig. 2G), with the exception of an ~50% increase in 18:2 CoA in the hypothalamus and cortex (see Fig. S2A to C in the supplemental material). This change is very

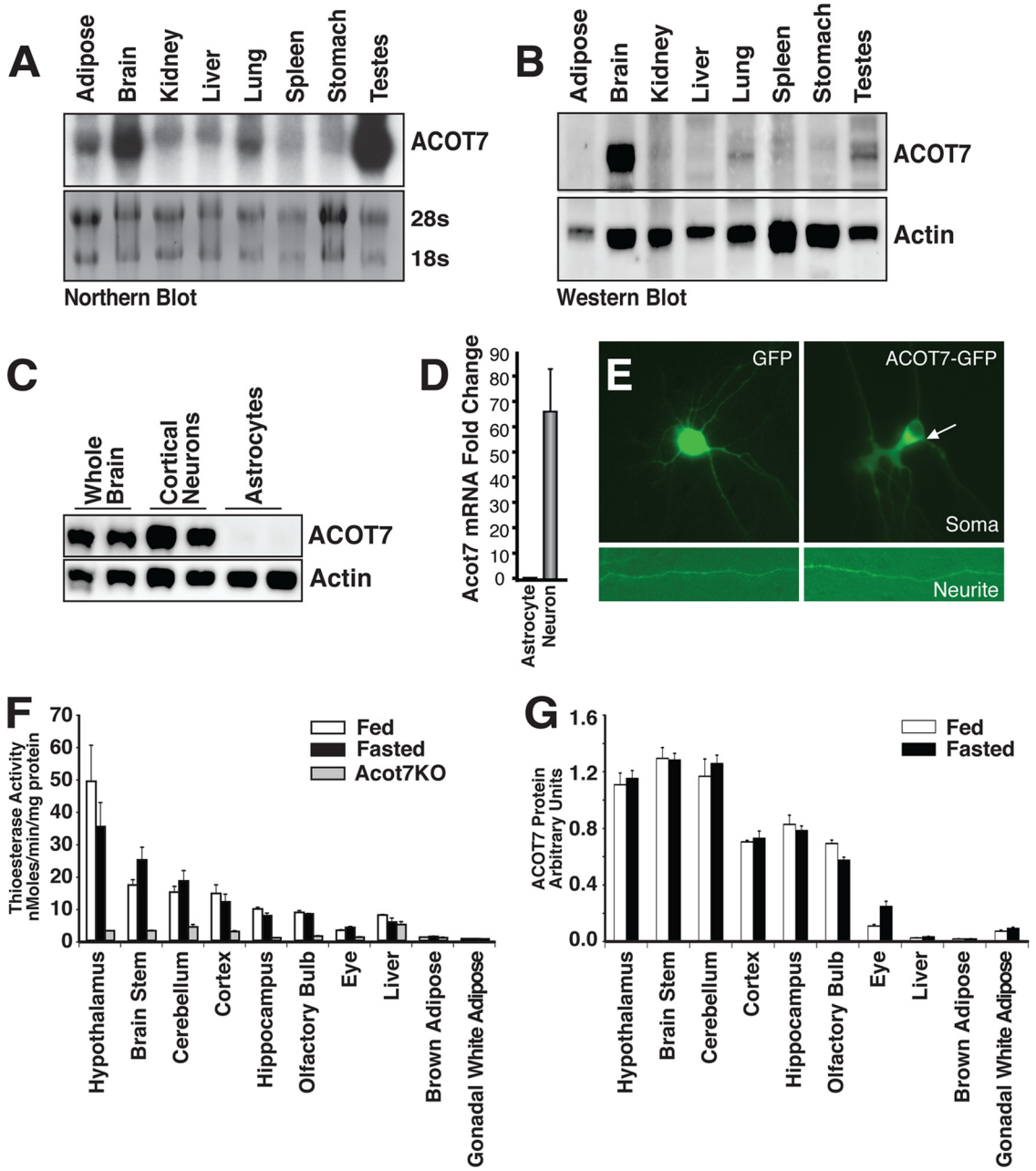

FIG 1 ACOT7 is highly and selectively expressed in neurons. (A) Northern blot tissue profiling of mouse *acot7* mRNA. (B) Western blot tissue profiling of mouse ACOT7. (C and D) Western blot (C) or real-time RT-PCR (D) of ACOT7 in cultured rat cortical astrocytes or cortical neurons. (E) Epifluorescence microscopy images of neurites and soma of primary cortical neurons expressing either GFP or ACOT7-GFP. (F and G) Total thioesterase activity (F) or ACOT7 protein abundance (G) measured from total homogenates prepared from fed or overnight-fasted male and female control and $Acot7^{-/-}$ mice; $n = 3$ to 4. Data represent averages ± standard errors of the means.

similar to that seen in brown adipose tissue of ACOT11 KO mice (24). Total brain coenzyme A, a product of the ACOT7 reaction, also did not change between control and $Acot7^{N-/-}$ mice (Fig. 2H). Therefore, we can conclude that ACOT7 is the major thioesterase in the brain; however, the loss of ACOT7 does not affect the steady-state concentration of long-chain acyl-CoAs or coenzyme A in the brain.

Neurometabolomic profiling reveals multiple roles for ACOT7 in regulating neuronal metabolism. We were surprised that the steady-state concentration of brain long-chain acyl-CoAs were not altered after removal of a seemingly important regulatory step in neural fatty acid metabolism. To gain a more thorough understanding about the metabolic consequence of deleting ACOT7, we performed unbiased neurometabolomic profiling of $Acot7^{N-/-}$ and control littermate brains after overnight fasting. The data showed many robust changes in fatty acid metabolites but also in carbohydrate (Fig. 3A) and glutamate metabolites (see Table S1 in the supplemental material). $Acot7^{N-/-}$ brains, com-

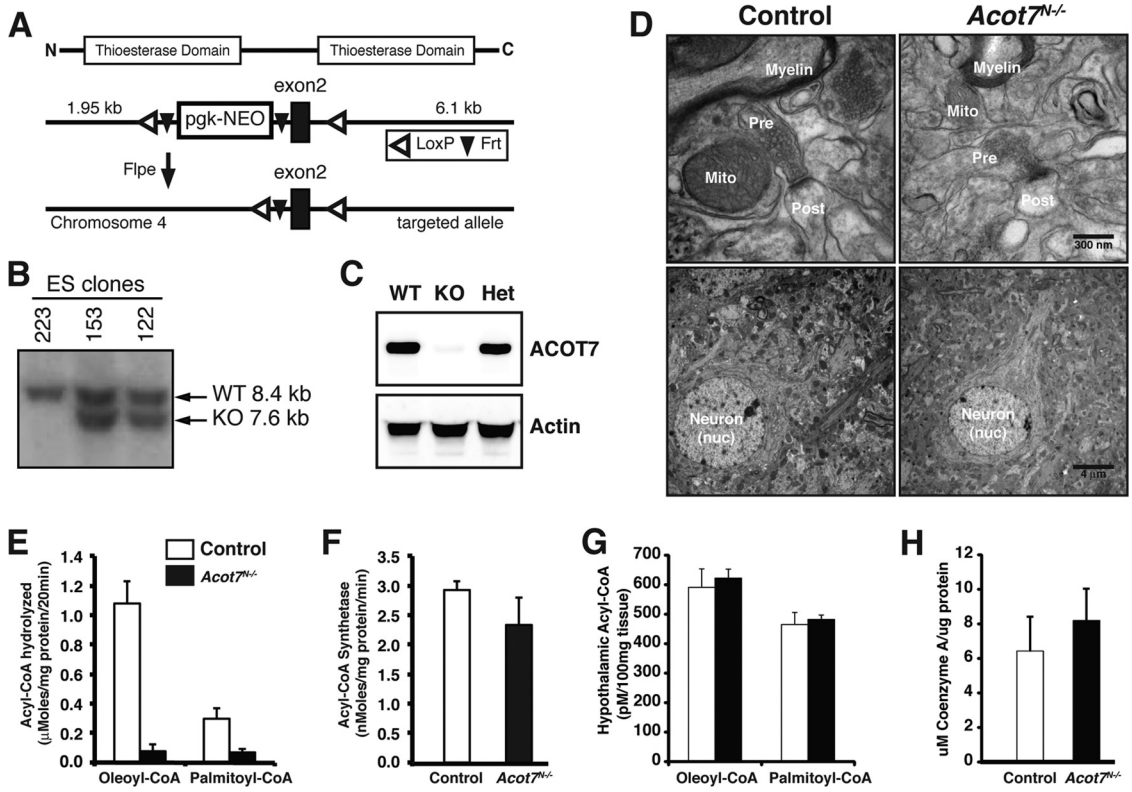

FIG 2 Generation of ACOT7 brain-specific knockout mice. (A) Gene targeting strategy. (B) Southern blot of ES cell clones showing correct targeting. (C) Western blot for mice with a brain-specific knockout of ACOT7. (D) Representative electron micrograph images of control and *Acot7*$^{N-/-}$ brains from fed mice. pre, presynaptic; post, postsynaptic; nuc, nucleus; mito, mitochondria. (E and F) Total long-chain acyl-CoA thioesterase (E) or total long-chain acyl-CoA synthetase (F) activity in homogenates from 3- to 4-month-old male and female control and *Acot7*$^{N-/-}$ brains; $n = 4$ to 6. (G and H) Hypothalamic long-chain acyl-CoA content (G) or brain coenzyme A content (H) from 3- to 4-month-old male and female control and *Acot7*$^{N-/-}$ mice; $n = 6$. Data represent averages ± standard errors of the means.

pared to controls, had an increase in long-chain acyl-CoA-dependent metabolites, including a 2.9-fold increase in oleoyl-carnitine, a 1.6-fold increase in β-hydroxybutyrate, and a 3.7-fold increase in sphingosine (Fig. 3B and C). These steady-state data suggest an increased long-chain acyl-CoA-dependent metabolic flux in *Acot7*$^{N-/-}$ brains. Strikingly, *Acot7*$^{N-/-}$ brains, compared to controls, had 1.2- to 2-fold increases in a majority of the profiled long-chain nonesterified fatty acids (Fig. 3D). This was surprising, since we would expect a reduction of long-chain nonesterified fatty acids with the loss of ACOT7. This increase, however, was concomitant with large increases in a majority of the profiled lysophospholipids, which, along with nonesterified fatty acids, comprise another product of phospholipase activity (Fig. 3E). Acyl-CoA thioesterase 7 does not hydrolyze fatty acids from phospholipids (41); however, some phospholipases have been shown to contain acyl-CoA thioesterase activity (42). Also, a mitochondrial acyl-CoA thioesterase (ACOT15) plays a role in remodeling cardiolipin (43). Together, these data are consistent with ACOT7 being a long-chain acyl-CoA thioesterase that regulates brain fatty acid metabolism but also suggest that it may have more specialized functions or regulation *in vivo*, such as in complex lipid remodeling.

As expected, since fatty acid metabolism is intertwined with many other metabolic pathways, the KO of ACOT7 affected the metabolism of other macronutrients. *Acot7*$^{N-/-}$ brain glucose was increased almost 2-fold, fructose-1,6-biphosphate was increased, and 3-phosphoglycerate was decreased, suggesting altered glucose metabolism (see Table S1 in the supplemental material). These data show that under fasting conditions, while ACOT7 does not affect the long-chain acyl-CoA steady-state concentration, it does regulate brain acyl-CoA-dependent metabolism. Together, these data suggest that ACOT7 plays a critical role in regulating multiple aspects of brain fatty acid and macronutrient metabolism and represents a critical metabolic node in neurons.

ACOT7 is required to regulate fasting-induced neuronal fatty acid metabolism. To confirm the steady-state metabolite data showing increases in *Acot7*$^{N-/-}$ brain free fatty acid content, we measured lipids from control and *Acot7*$^{N-/-}$ mice under both fed and fasting conditions. After overnight fasting, *Acot7*$^{N-/-}$ brain total nonesterified fatty acid content, compared to that of controls, was significantly increased (Fig. 4A). In addition to increased free fatty acids, we found that *Acot7*$^{N-/-}$ brains have increased phospholipid and triacylglycerol content but no change in cholesterol (Fig. 4B to D). Changes in triacylglycerol content in the brain were likely in ependymal cells (44). Because the metabolite data suggested an increase in phospholipase activity, we measured brain cytosolic phospholipase A_2 activity in control and *Acot7*$^{N-/-}$ brains. Brain cytosolic phospholipase A2 (cPLA$_2$) activity was unchanged in fed *Acot7*$^{N-/-}$ mice compared to that in

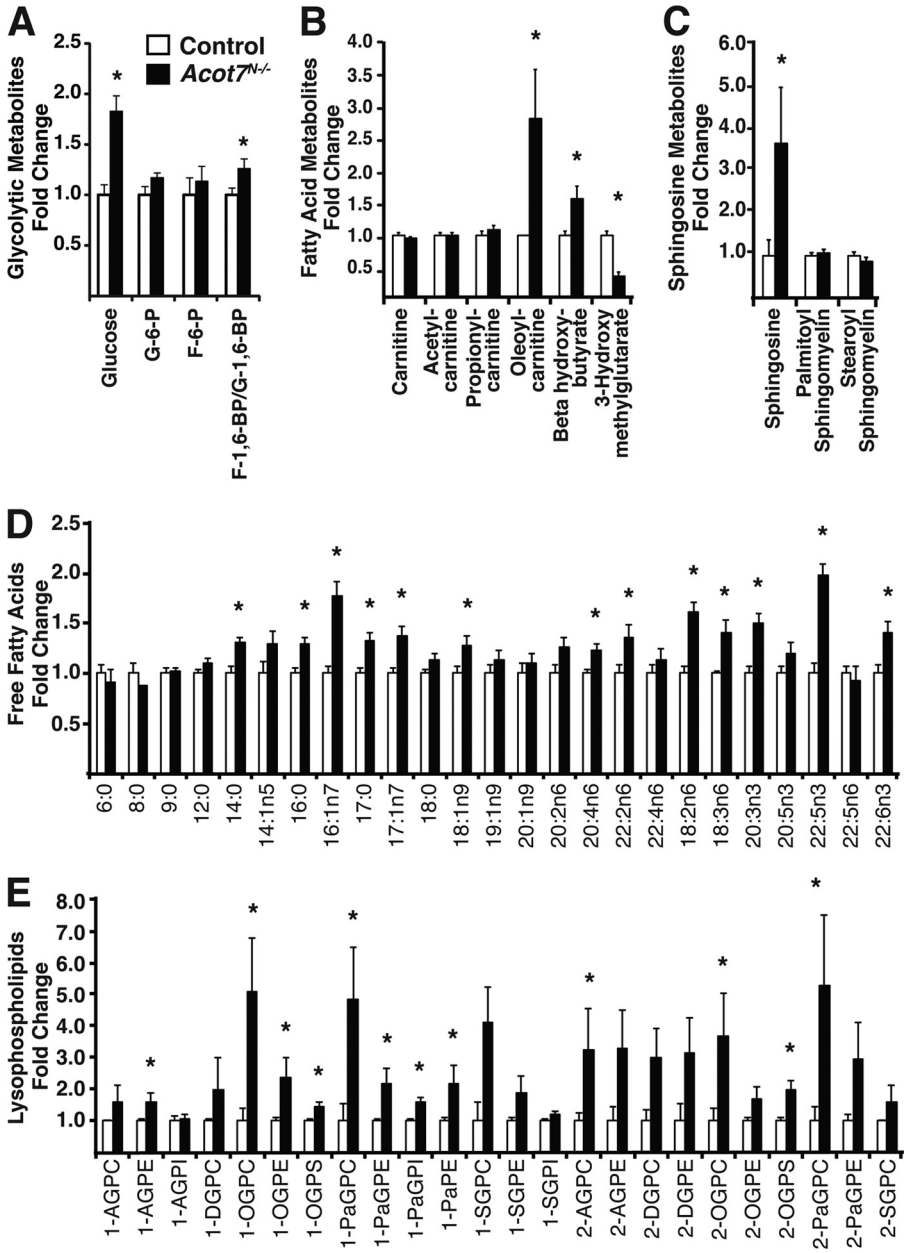

FIG 3 ACOT7 regulates brain cellular fatty acid metabolism. Total brain glycolytic metabolites (A), fatty acid metabolites (B), sphingosine metabolites (C), free fatty acids (D), or lysophospholipids (E) from overnight-fasted 3- to 4-month-old male and female control and *Acot7*$^{N-/-}$ mice are analyzed; $n = 7$. Abbreviations: G, glucose; F, fructose (A); A, arachidonoyl; G, glycerol; P, phospho; C, choline; I, inositol; E, ethanolamine; D, docosahexaenoyl; O, oleoyl; S, stearoyl; Pa; palmitoyl (E). Data represent averages ± standard errors of the means. "*" indicates $P \leq 0.05$ by Welch's two-sample *t* test comparing controls to *Acot7*$^{N-/-}$ mice.

controls; however, under fasting conditions, $cPLA_2$ activity increased in *Acot7*$^{N-/-}$ brains compared to that in controls (Fig. 4E), suggesting that the increased free fatty acids and lysophospholipids may be due in part to increased $cPLA_2$ activity. Interestingly, of the metabolites we measured, none were different between control and *Acot7*$^{N-/-}$ mice under fed conditions, indicating that ACOT7 activity is critical for regulating fatty acid flux into lipids during the fasting state, when circulating free fatty acids are elevated.

To better understand how metabolic flux was changed in *Acot7*$^{N-/-}$ brains, we performed tracer studies using radiolabeled metabolites in freshly isolated brain slices from overnight-fasted mice. In *Acot7*$^{N-/-}$ slices, compared to results for controls, we observed a nonsignificant decrease in the rate of [1-^{14}C]oleate oxidation (Fig. 4F). The rate of glucose oxidation into CO_2 was increased 20% (Fig. 4G) for *Acot7*$^{N-/-}$ mice compared to that for controls. The increase in glucose oxidation may be due to increased excitability of *Acot7*$^{N-/-}$ neurons or to compensate for the decreased FA oxidation. The rate of incorporation of [1-^{14}C]oleate into complex lipids was increased in *Acot7*$^{N-/-}$ brain slices compared to that in controls (Fig. 4H). The rate of *de novo* fatty acid synthesis, measured by the rate of [^{3}H]acetate in-

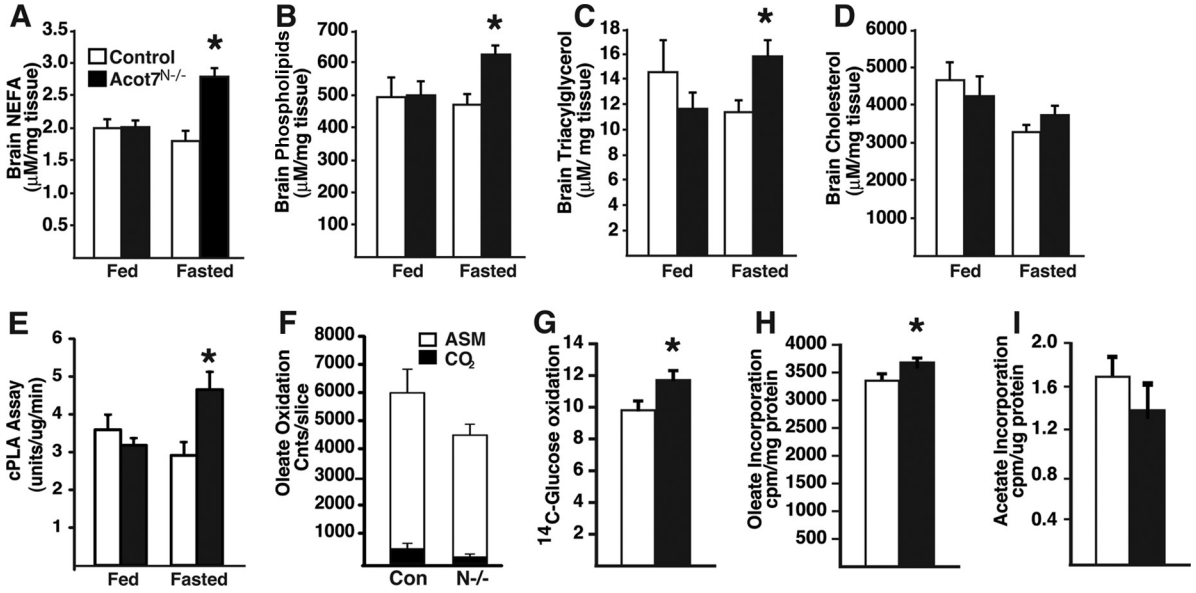

FIG 4 ACOT7 inhibits fasting-induced lipid metabolism. (A to D) Brain nonesterified fatty acids (A), phospholipids (B), TAG (C), or cholesterol content (D) in lipid fractions derived from 3- to 4-month-old male and female control and *Acot7*$^{N-/-}$ brains with or without overnight fasting; $n = 6$ to 8. (E) Cytosolic phospholipase A2 activity in 3- to 4-month-old male and female control and *Acot7*$^{N-/-}$ brains with or without overnight fasting; $n = 6$. (F to I) Oleate oxidation to CO_2 and acid-stable metabolites (ASM) (F), glucose oxidation (G), oleate incorporation into lipids (H), or acetate incorporation into lipids (I) in brain slices derived from overnight-fasted 3- to 6-month-old male and female control and *Acot7*$^{N-/-}$ mice; $n = 6$ to 8. White bars represent data from control mice, and black bars represent data from *Acot7*$^{N-/-}$ mice, except in panel F (Con, control; N-/-, *Acot7*$^{N-/-}$; Cnts, counts). Data represent averages ± standard errors of the means. "*" indicates $P \leq 0.05$ by two-tailed Student's *t* test comparing controls to *Acot7*$^{N-/-}$ mice.

corporation into the lipid fraction, was unchanged between control and *Acot7*$^{N-/-}$ brain slices (Fig. 4I). These data suggest that the loss of neuronal ACOT7 increases fatty acid flux into complex lipids and increases $cPLA_2$ activity. These data support the increase in phospholipid and lysophospholipid content observed in fasted *Acot7*$^{N-/-}$ brain. Furthermore, the role of ACOT7 in regulating neuronal fatty acid metabolism is most important during fasting, when circulating free fatty acids are high.

Loss of ACOT7 results in a reduction in lean mass coupled with systemic dyslipidemia. The loss of ACOT7 in the nervous system had no effect on body weight (Fig. 5A), liver, kidney, or brown adipose tissue weight (Fig. 5B); however, the weights of inguinal and gonadal adipose depots were 50% and 39% greater, respectively, in the *Acot7*$^{N-/-}$ mice (Fig. 5B). Because the central administration of fatty acids has been shown to suppress food intake via increased long-chain acyl-CoAs (45, 46), we monitored food intake for individually housed mice. *Acot7*$^{N-/-}$ mice fed a chow diet had no change in food intake. The mRNA abundance of the hypothalamic neuropeptides Agrp, Pomc, and Cart were not different between genotypes, whereas neuropeptide Y (Npy) mRNA abundance was modestly increased, ~20%, in the *Acot7*$^{N-/-}$ mice (see Fig S3C in the supplemental material). To test fatty acid-induced changes in the regulation of food intake, we fed mice a high-fat diet and found no change in food intake between genotypes (Fig. 5C). Whole-body nuclear magnetic resonance (NMR) analysis of control and *Acot7*$^{N-/-}$ mice confirmed a 52 to 46% increase in adiposity in male and female mice (Fig. 5D). In concordance with an unaltered body weight, NMR data showed that lean mass was 8 to 5% lower in *Acot7*$^{N-/-}$ male and female mice (Fig. 5E) without changes in fasting serum creatine kinase (Table 1). Gene expression analysis of fasting *Acot7*$^{N-/-}$ gonadal adipose tissue, compared to results for controls, showed a decrease in mRNA abundance of the fatty acid oxidation gene medium-chain acyl-CoA dehydrogenase (Mcad) and a decrease mRNA abundance of the Pgc1α and Cpt1b brown adipocyte marker genes within gonadal white adipose tissue (GWAT) (Fig. 5F). These data suggested that increased adipose mass may be due to reduced oxidative capacity in adipose coupled with a redistribution of lean mass to adipose.

In addition to increased adipose stores, the *Acot7*$^{N-/-}$ mice have 46% more hepatic triacylglycerol (TAG) than control mice after an overnight fast (Fig. 5G to J). Liver cholesterol and circulating cholesterol, glycerol, and glucose were similar between the control and *Acot7*$^{N-/-}$ mice after overnight fasting; however, circulating free fatty acids, β-hydroxybutryate, and TAG were 49%, 71%, and 57% higher, respectively, in the *Acot7*$^{N-/-}$ mice (Fig. 5 and Table 1). Liver mRNA abundance of fatty acid synthase (Fasn) and stearoyl-CoA desaturase 1 (Scd1) and the apolipoprotein C3 (Apoc3) genes were increased by 2.4-, 2.25-, and 1.75-fold, respectively, in *Acot7*$^{N-/-}$ mice compared to that in control liver (Fig. 5K). There was no change in mRNA abundance of gluconeogenic and oxidative phosphorylation genes; however, we did observe an increase in both carnitine palmitoyltransferases 1b and 1a (Cpt1b and Cpt1a) in *Acot7*$^{N-/-}$ livers (Fig. 5K and L). While the mRNA of mitochondrial oxidative phosphorylation genes, as well as mitochondrial DNA content, were not upregulated in the *Acot7*$^{N-/-}$ livers (Fig. 5L; see also Fig. S3A in the supplemental material), the protein abundance of NADH dehydrogenase (ubiquinone) 1 beta subcomplex 8 and succinate dehydrogenase complex subunit B were increased (Fig. 5M and N). These data suggest that *Acot7*$^{N-/-}$ livers upregulated oxidative proteins, as well as the mRNA abundance of fatty acid synthesis and lipid

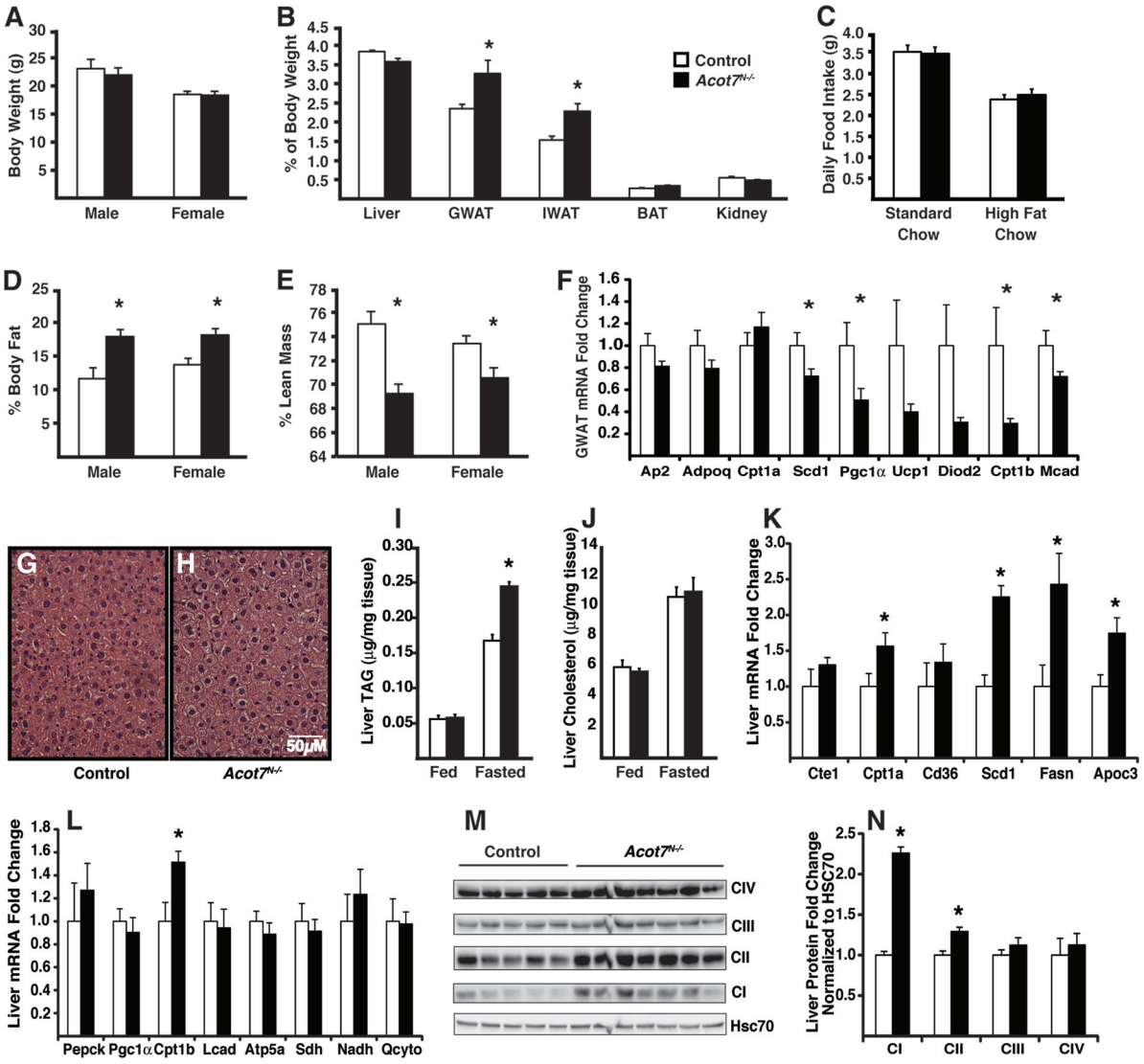

FIG 5 Dysregulated peripheral lipid metabolism and storage in *Acot7*$^{N-/-}$ mice. (A) Body weight of control or *Acot7*$^{N-/-}$ 5- to 6-month-old male and female mice; $n = 5$ to 7. (B) Organ weight, expressed as a percentage of body weight, for 5- to 6-month-old female control and *Acot7*$^{N-/-}$ mice; $n = 5$ to 7. (C) Food intake of 4-month-old male mice; $n = 6$ to 8. (D and E) Percent body fat (D) or lean mass (E) in 3- to 4-month- old male and female mice; $n = 7$ to 10. (F) Gonadal white adipose mRNA abundance for oxidative genes from 5- to 6-month old female control and *Acot7*$^{N-/-}$ mice; $n = 6$. (G to J) H&E-stained liver from overnight-fasted mice (G and H) or liver TAG (I) or liver cholesterol (J) content from 5- to 6-month-old male and female control and *Acot7*$^{N-/-}$ mice under fed or overnight-fasted conditions; $n = 5$ to 8. (K and L) mRNA abundance in liver; $n = 5$ to 7. (M and N) Western blot images (M) or quantification of mitochondrial oxidative phosphorylation proteins (N) from 5- to 6-month-old female control and *Acot7*$^{N-/-}$ livers; $n = 5$ to 7. Data represent averages ± standard errors of the means. "*" indicates $P \leq 0.05$ by a two-tailed Student *t* test comparing controls to *Acot7*$^{N-/-}$ mice.

secretion genes, which is concordant with increased circulating β-hydroxybutryate and TAG (Table 1). We suspect that the excess circulating fatty acids accumulate due to increased adipose stores in the *Acot7*$^{N-/-}$ mice, and that these fatty acids are taken up by the liver for storage, conversion to ketones, and packaging into very low density lipoprotein (VLDL), for which the *Acot7*$^{N-/-}$ liver has upregulated the necessary machinery. These data suggest that while glucose homeostasis is maintained, whole-body fatty acid metabolism is dysregulated with the loss of neuronal ACOT7.

***Acot7*$^{N-/-}$ mice exhibit exaggerated stimulus-evoked behavior and physiology.** Free fatty acids are known to elicit a response from a subset of neurons in culture (47, 48), and when injected into the lateral ventricles, free fatty acids affect animal behavior and physiology (45, 46). Therefore, we tested whether a loss of ACOT7 would effect metabolic adaptations controlled, in part, by the nervous system. First, *Acot7*$^{N-/-}$ mice had no differences in body weight or food intake over time (Fig. 5A and C). We next monitored cage activity and energy expenditure (VO_2 and VCO_2) of *Acot7*$^{N-/-}$ and control mice in response to normal circadian rhythms and to overnight fasting in metabolic chambers. While the *Acot7*$^{N-/-}$ respiratory exchange ratio was similar to that for control mice throughout the experiment (data not shown), during the 24-h fasting period, the *Acot7*$^{N-/-}$ mice exhibited acute hyperactivity and corresponding elevated energy expenditure compared to controls (Fig. 6A to D). In *Acot7*$^{N-/-}$ mice, acute spikes in energy

TABLE 1 Serum metabolite values and body temperature for 3- to 5-month-old overnight-fasted control and *Acot7*$^{N-/-}$ male and female mice[a]

Parameter	Value for group (n[b])			
	Female		Male	
	Control (5)	*Acot7*$^{N-/-}$ (6)	Control (7)	*Acot7*$^{N-/-}$ (8)
β-HB (mmol/liter)	1.8 ± 0.2	3.1 ± 0.4*	1.2 ± 0.2	1.9 ± 0.2*
TAG (mg/dl)	9.8 ± 1.9	22.7 ± 4.9*	25.6 ± 3.8	36.1 ± 1.4*
Glycerol (mg/dl)	24.8 ± 4.4	21.9 ± 1.3	24.6 ± 3.9	29.8 ± 2.6
NEFA (mmol/liter)	0.84 ± 0.06	1.17 ± 0.1*	0.75 ± 0.18	0.8 ± 0.12
Cholesterol (mg/dl)	71.6 ± 2.7	64.8 ± 6.1	94.3 ± 7.3	102.2 ± 9.0
Glucose (mg/dl)	66 ± 5	68 ± 3	65 ± 2	70 ± 6
Body temp (°C)	34.5 ± 0.5	36.5 ± 0.3*	34.7 ± 0.3	35.7 ± 0.4
Creatine kinase (U/liter)	7,738 ± 370	6,934 ± 1,399	9,404 ± 568	9,437 ± 698

[a] β-HB, beta-hydroxybutryate; TAG, triacylglycerol; NEFA, nonesterified fatty acids. Data represent averages ± SE. "*" indicates $P \leq 0.05$ by a two-tailed Student t test comparing controls to *Acot7*$^{N-/-}$ mice within sex.
[b] n, no. of mice.

expenditure during the light phase after overnight fasting did not correlate with increased physical activity (Fig. 6A to D), suggesting that the loss of neuronal ACOT7 increases energy expenditure via heat production the morning after an overnight fast. We next monitored body temperature of control and *Acot7*$^{N-/-}$ mice throughout the day under fed or fasting conditions and found no change in body temperature between genotypes, with the exception of a significant increase in body temperature for *Acot7*$^{N-/-}$ mice the morning after overnight fasting (Table 1). To confirm increased heat production in the *Acot7*$^{N-/-}$ mice, we challenged the mice with a cold (4°C) environment for 5 h with or without an overnight fast and found that *Acot7*$^{N-/-}$ mice were able to maintain a higher body temperature than the controls (Fig. 6E). Adrenergic-responsive genes were induced similarly between genotypes by acute cold exposure, suggesting that the elevated body temperature in the *Acot7*$^{N-/-}$ mice is not due to altered adrenergic input or to an altered brown adipose tissue (BAT) adrenergic response (see Fig. S3B in the supplemental material). Thus, the loss of neuronal ACOT7 increased physical activity and energy expenditure during food deprivation. Furthermore, *Acot7*$^{N-/-}$ mice had elevated thermogenesis during cold exposure, suggestive of a hyperactive neural response to physiological challenges. Increased energy expenditure following an overnight fast is a phenomenon also observed in patients with the neurodegenerative disease amyotrophic lateral sclerosis (ALS) (49).

To further explore the hyperactive responsiveness, we examined the prepulse inhibition (PPI) of *Acot7*$^{N-/-}$ mice via an unconditioned acoustic stimulus. With proper sensorimotor gating, a weak prepulse received prior to a higher acoustic pulse will reduce the startle response compared to the startle response elicited by a single high acoustic stimulus. *Acot7*$^{N-/-}$ mice exhibited a defective PPI response, suggesting impaired sensorimotor gating and improper neuronal activity (Fig. 6F). Together, these data support the conclusion that *Acot7*$^{N-/-}$ mice exhibit a hyperexcitability to specific stimulus-evoked behaviors.

Loss of ACOT7 results in a progressive neurodegenerative phenotype. The loss of lean mass, hypermetabolism, hepatic steatosis, dyslipidemia, and hyperexcitability in *Acot7*$^{N-/-}$ mice is reminiscent of findings for patients with motor neuron dysfunction, such as amyotrophic lateral sclerosis (50). Furthermore, the fasting-induced increases in seemingly toxic lipid metabolites and PLA activity in the brain would suggest a neuroprotective role for ACOT7. Therefore, we tested motor coordination in *Acot7*$^{N-/-}$ mice via an accelerating rotarod treadmill. Aged *Acot7*$^{N-/-}$ mice had a significant defect in their ability to remain on the rotarod, suggestive of a neurological defect (Fig. 7A). We also tested neurodegeneration via scoring the performance of control and *Acot7*$^{N-/-}$ mice during a ledge and clasp test, as well as monitoring their gate and kyphosis. *Acot7*$^{N-/-}$ mice had a greater score than controls, again indicating a neurological defect (Fig. 7B). The mice were subjected to open field tests to assess both anxiety and spontaneous motor activity. The open field data suggest that *Acot7*$^{N-/-}$ mice do not have excessive anxiety, because the proportion of time spent in the center of the open field apparatus was similar to that of the control mice (data not shown); however, the *Acot7*$^{N-/-}$ mice, compared to the control mice, had significantly fewer total beam breaks (or activity), consistent with locomotor defects (Fig. 7C). We next examined neuronal density by measuring the width of the neuronal granular cell layer in the cerebellum of Nissl-stained histological sections and found that *Acot7*$^{N-/-}$ mice, compared to controls, have significantly lower cerebellar neuronal cell density, suggesting neurodegeneration in *Acot7*$^{N-/-}$ mice (Fig. 7D). Motor control is coordinated by the cerebellum and motor neurons; therefore, we looked at cerebellar GFAP expression via Western blotting as an additional measure of reactive gliosis and neurodegeneration in 8-, 24-, and 40-week-old mice. Eight-week-old *Acot7*$^{N-/-}$ mice did not have enhanced GFAP expression; however, 24- and 40-week-old *Acot7*$^{N-/-}$ mice did have significantly upregulated GFAP expression, indicating age-dependent neurodegeneration (Fig. 7E and F). This was additionally confirmed by the upregulation of GFAP mRNA expression in 40-week-old *Acot7*$^{N-/-}$ cerebellum (Fig. 7G).

One cause of familial ALS is mutations in superoxide dismutase 1 (SOD1), which has led to great interest in understanding the role and dysregulation of oxidative metabolism in neurons. Therefore, we examined proteins in *Acot7*$^{N-/-}$ mice that were shown to be aberrantly expressed in models of ALS (51). Consistent with other models of neurodegeneration, *Acot7*$^{N-/-}$ mice had an upregulation of voltage-dependent anion channel 1 (VDAC1), cytochrome *c* oxidase (CoxIV), and superoxide dismutase 2 (SOD2) (Fig. 7H and I) (52). These data lend further evidence that ACOT7 is required for neuroprotection.

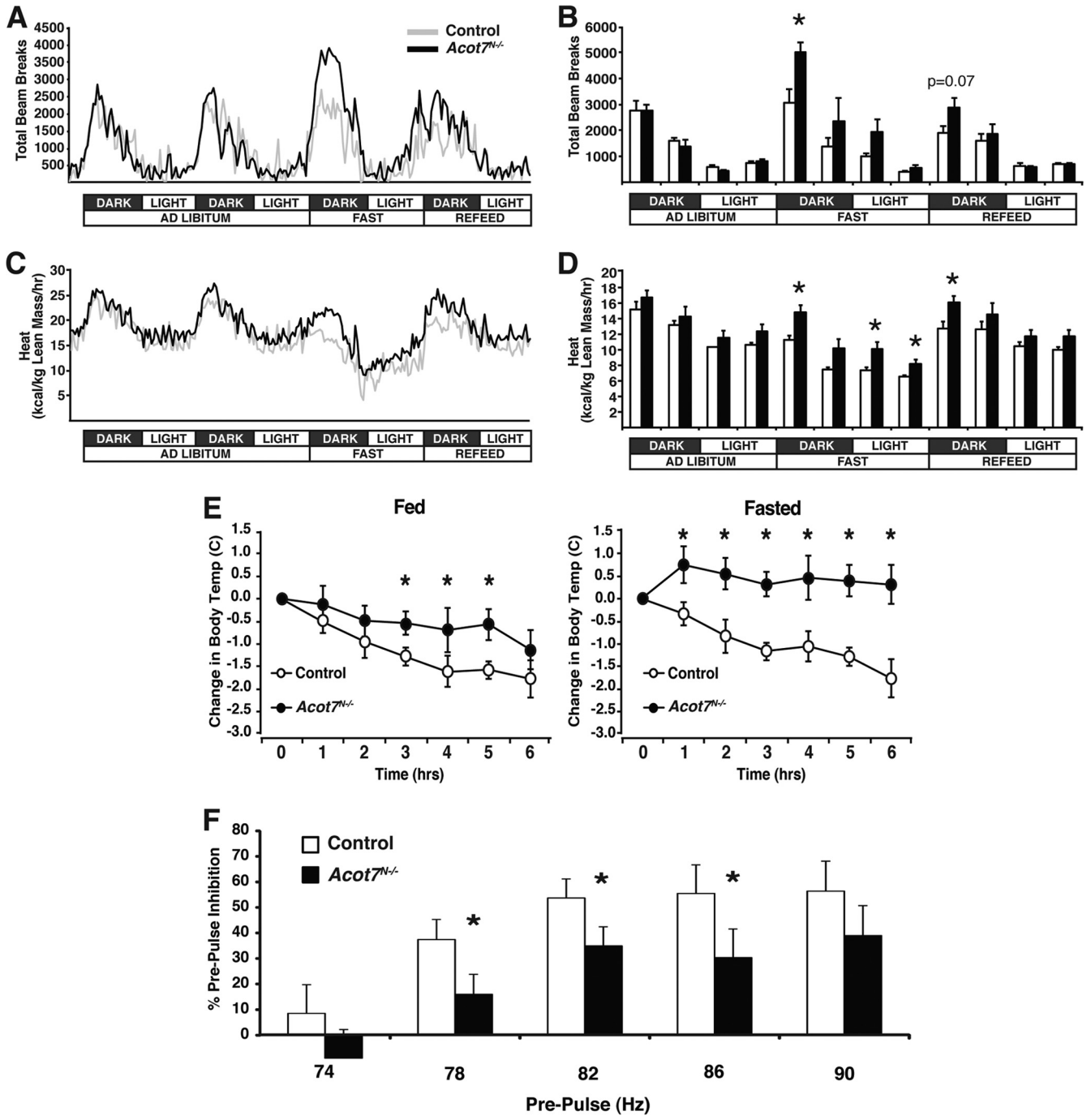

FIG 6 *Acot7*$^{N-/-}$ mice show maladaptive response to stimulus-evoked behavior. (A and B) Movement of 3- to 4-month-old control and *Acot7*$^{N-/-}$ female mice, monitored by CLAMS, graphed over time (A) or in 6-h binned increments (B); $n = 5$ to 7. (C and D) Energy expenditure of control and *Acot7*$^{N-/-}$ female mice, monitored by CLAMS and graphed over time (C) or in 6-h binned increments (D); $n = 5$ to 7. (E) Change in body temperature of 5- to 6-month-old male and female control and *Acot7*$^{N-/-}$ mice during a 6-h cold exposure with or without overnight fasting. (F) Prepulse inhibition from acoustic startle response in 3- to 5-month-old male and female control and *Acot7*$^{N-/-}$ mice; $n = 17$ to 20. Data represent averages ± standard errors of the means. "*" indicates $P \leq 0.05$ by a two-tailed Student *t* test comparing controls to *Acot7*$^{N-/-}$ mice.

DISCUSSION

The only tissue that is more lipid rich than the brain is adipose tissue. Fatty acids, particularly those that cannot be made *de novo*, such as docosahexaenoic acid, are enriched in the brain and are important for neural development and function. An imbalanced lipid composition can have dire consequences for brain function; however, how the brain derives and maintains its unique balance of lipids remains unclear. Here we have shown that ACOT7, also known as brain acyl-CoA hydrolase, is required to maintain neuronal fatty acid homeostasis *in vivo* and is critical for counterbal-

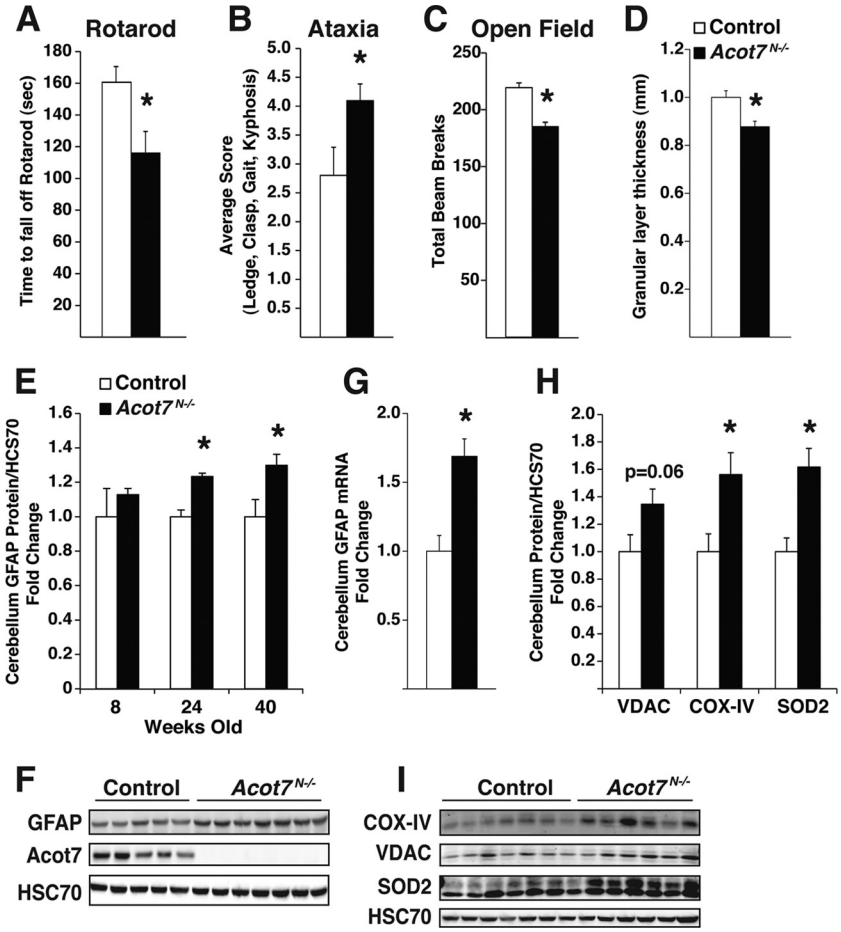

FIG 7 Loss of ACOT7 results in progressive neurodegeneration and neurological dysfunction. (A and B) Rotarod performance (A) or cerebellar ataxia assessment (B) for 10-month-old control and *Acot7*$^{N-/-}$ male mice, average of 3 to 5 trials blinded to the observer; $n = 6$ to 8. (C) Total movement in open field apparatus was monitored over a 40-min period for 3- to 5-month-old male control and *Acot7*$^{N-/-}$ mice; $n = 8$ to 10. (D) Cerebellar granular cell layer thickness, as a ratio of lobule width, was measured for Nissl-stained 10-month-old control and *Acot7*$^{N-/-}$ male mice blinded to the observer; $n = 6$ to 8. (E and F) Quantification (E) or representative Western blots (F) of GFAP, normalized to HSC70, from male and female control and *Acot7*$^{N-/-}$ cerebellum of 8-, 24-, and 40-week-old mice; $n = 3$ to 7. (G) Cerebellum *Gfap* mRNA abundance, relative to that of *Gapdh*, from 5- to 6-month-old female control and *Acot7*$^{N-/-}$ mice; $n = 6$. (H and I) Quantification (H) or representative Western blots (I) of VDAC, CoxIV, and SOD2 in cerebellum of 24-week-old female control and *Acot7*$^{N-/-}$ mice; $n = 6$ to 8. Data represent averages ± standard errors of the means. "*" indicates $P \leq 0.05$ by a two-tail Student *t* test comparing controls to *Acot7*$^{N-/-}$ mice.

ancing fasting-induced metabolism of fatty acids in neurons. Furthermore, the loss of ACOT7 results in multiple defects in neural metabolism, leading to progressive neurodegeneration. Counterregulating fatty acid metabolism via acyl-CoA hydrolysis is uniquely important in neurons, because they have a limited capacity for neutral lipid storage and mitochondrial fatty acid beta oxidation, which are two major pathways for long-chain acyl-CoA metabolism. The expression of ACOT7 in neurons not only provides metabolic balance but also diverts the metabolic burden from nonreplicative neurons onto the glia.

ACOT7 was cloned and characterized for its thioesterase activity, substrate preference, and tissue distribution (53, 54). ACOT7 has five alternative start sites that have unique expression patterns across tissues and are found in both the cytosol and mitochondria (37), although our targeting strategy removes all of these putative active products. We found ACOT7 to be highly abundant in the cytosol of neurons, with very limited detection of the protein elsewhere. ACOT7 was also shown to be expressed in activated macrophages, and the overexpression of ACOT7 in macrophages decreased prostaglandin D2 and E2 production (40). Eicosanoid synthesis uniquely utilizes free arachidonate rather than arachidonoyl-CoA, and while we did see increases in free fatty acid content, we did not observe changes in prostaglandin D2 or E2 content in *Acot7*$^{N-/-}$ brains (see Table S1 in the supplemental material). Thus, it is possible that ACOT7 plays unique roles in regulating cellular metabolism and behaves in a cell-type-specific manner.

The biochemical function of acyl-CoA thioesterases presents a conundrum in fatty acid metabolism. It would be predicted that ACOTs would antagonize the use of fatty acids and result in an apparent futile cycling via fatty acid activation/deactivation. In support of this notion, we see an increase in acyl-CoA-dependent pathways; however, we also see a paradoxical increase in brain free fatty acids and lysophospholipids. These data would not be predicted from a simple antagonization model. The loss of a related mammalian thioesterase, ACOT15, also results in defects in mitochondrial membrane remodeling (43). Furthermore, the expression of the putative acyl-CoA thioesterase from *Bacillus subtilis*

(YkhA) was correlated with increased membrane remodeling (55). Therefore, thioesterases may play a critical role in the acylation/reacylation process of membrane remodeling. Other thioesterases have also been implicated in the regulation of fatty acid metabolism. ACOT1 is a peroxisome proliferator-activated receptor alpha (PPAR-alpha) target gene and is highly upregulated in the liver during fasting, which is paradoxical because fasting liver is performing a great deal of acyl-CoA-dependent fatty acid oxidation (56–58). The loss of ACOT11, which is highly expressed in brown fat, resulted in increased energy expenditure via thermogenesis, a process requiring acyl-CoA-dependent fatty acid oxidation (24). Data from multiple models of thioesterase deficiencies, including the findings herein, show multiple metabolic derangements. These data suggest that the role of thioesterases in cellular metabolism and regulation likely involves complex interplay between numerous interacting pathways that have yet to be fully elucidated.

To date there have not been mutations found in ACOT7 that have been associated with neurological disease; however, ACOT activity was shown to be absent in postmortem brain tissue of people suffering from mesial temporal lobe epilepsy, a disorder of neuronal hyperexcitability (59). Also, neural ACOT7 was shown to be regulated transcriptionally by neuronal activation (60) and ketogenic feeding (61). This is important because ketogenic diets increase circulating ketones and free fatty acids (62), and these diets are used therapeutically as an antiepileptic treatment. Patients with schizophrenia, which is also characterized by neuronal hyperexcitability and suppressed prepulse inhibition, were shown to have upregulated expression of ACOT7 as well (63). ACOT7 protein abundance in synaptosomes was increased ~5-fold, compared to that for controls, in mice expressing the neuroprotective slow Wallerian degeneration (Wld^s) gene, suggesting, along with the data herein, that ACOT7 may be an essential neuroprotective component in these mice (64). These observations suggest that ACOT7 is intimately involved in coordinating intracellular neurometabolism with the energetically demanding process of neuronal activity to prevent neurodegeneration.

In summary, we show that ACOT7 is an important regulator of neural metabolism and that its loss results in multiple defects in the regulation of fatty acid metabolism in the brain. The biochemical and physiological consequences of a loss of ACOT7 are greatly exacerbated by fasting, a time when circulating free fatty acids from lipolysis are elevated. The consequence of a loss of ACOT7 is exaggerated stimulus-evoked behavior and increased neurodegeneration, which in turn results in multiple physiological derangements. These data show that ACOT7 is an important regulator in neurometabolism that protects neurons against the damaging effects of fatty acid excess.

ACKNOWLEDGMENTS

We thank Susan Aja for assistance with the metabolic cage studies, Jenna Leser for assistance with mouse motor coordination experiments, and Mikhail Pletnikov for advice and discussions on mouse behavioral assays.

J.M.E. was supported by an interdepartmental training program in cellular and molecular endocrinology (T32DK007751). This work was supported by the American Heart Association (SDG2310008 to M.J.W. and SDG2260721 to G.W.W.), the National Institutes of Health (NS072241 to M.J.W. and DK084171 to G.W.W.), and Baltimore Diabetes Research and Training Center grant P60DK079637.

We have no competing financial interests.

REFERENCES

1. **Calon F, Lim GP, Yang F, Morihara T, Teter B, Ubeda O, Rostaing P, Triller A, Salem N, Jr, Ashe KH, Frautschy SA, Cole GM.** 2004. Docosahexaenoic acid protects from dendritic pathology in an Alzheimer's disease mouse model. Neuron **43**:633–645.
2. **Sharon R, Bar-Joseph I, Frosch MP, Walsh DM, Hamilton JA, Selkoe DJ.** 2003. The formation of highly soluble oligomers of alpha-synuclein is regulated by fatty acids and enhanced in Parkinson's disease. Neuron **37**: 583–595.
3. **Ellis CE, Murphy EJ, Mitchell DC, Golovko MY, Scaglia F, Barcelo-Coblijn GC, Nussbaum RL.** 2005. Mitochondrial lipid abnormality and electron transport chain impairment in mice lacking alpha-synuclein. Mol. Cell. Biol. **25**:10190–10201.
4. **Liu R, Li B, Flanagan SW, Oberley LW, Gozal D, Qiu M.** 2002. Increased mitochondrial antioxidative activity or decreased oxygen free radical propagation prevent mutant SOD1-mediated motor neuron cell death and increase amyotrophic lateral sclerosis-like transgenic mouse survival. J. Neurochem. **80**:488–500.
5. **Kim YJ, Nakatomi R, Akagi T, Hashikawa T, Takahashi R.** 2005. Unsaturated fatty acids induce cytotoxic aggregate formation of amyotrophic lateral sclerosis-linked superoxide dismutase 1 mutants. J. Biol. Chem. **280**:21515–21521.
6. **Lee Y, Morrison BM, Li Y, Lengacher S, Farah MH, Hoffman PN, Liu Y, Tsingalia A, Jin L, Zhang PW, Pellerin L, Magistretti PJ, Rothstein JD.** 2012. Oligodendroglia metabolically support axons and contribute to neurodegeneration. Nature **487**:443–448.
7. **Vos M, Esposito G, Edirisinghe JN, Vilain S, Haddad DM, Slabbaert JR, Van Meensel S, Schaap O, De Strooper B, Meganathan R, Morais VA, Verstreken P.** 2012. Vitamin K2 is a mitochondrial electron carrier that rescues pink1 deficiency. Science **336**:1306–1310.
8. **Diaz-Castro B, Pintado CO, Garcia-Flores P, Lopez-Barneo J, Piruat JI.** 2012. Differential impairment of catecholaminergic cell maturation and survival by genetic mitochondrial complex II dysfunction. Mol. Cell. Biol. **32**:3347–3357.
9. **Chakravarthy MV, Zhu Y, Lopez M, Yin L, Wozniak DF, Coleman T, Hu Z, Wolfgang M, Vidal-Puig A, Lane MD, Semenkovich CF.** 2007. Brain fatty acid synthase activates PPARalpha to maintain energy homeostasis. J. Clin. Invest. **117**:2539–2552.
10. **He W, Lam TK, Obici S, Rossetti L.** 2006. Molecular disruption of hypothalamic nutrient sensing induces obesity. Nat. Neurosci. **9**:227–233.
11. **Loftus TM, Jaworsky DE, Frehywot GL, Townsend CA, Ronnett GV, Lane MD, Kuhajda FP.** 2000. Reduced food intake and body weight in mice treated with fatty acid synthase inhibitors. Science **288**:2379–2381.
12. **Wang H, Astarita G, Taussig MD, Bharadwaj KG, DiPatrizio NV, Nave KA, Piomelli D, Goldberg IJ, Eckel RH.** 2011. Deficiency of lipoprotein lipase in neurons modifies the regulation of energy balance and leads to obesity. Cell Metab. **13**:105–113.
13. **Wolfgang MJ, Kurama T, Dai Y, Suwa A, Asaumi M, Matsumoto S, Cha SH, Shimokawa T, Lane MD.** 2006. The brain-specific carnitine palmitoyltransferase-1c regulates energy homeostasis. Proc. Natl. Acad. Sci. U. S. A. **103**:7282–7287.
14. **Reamy AA, Wolfgang MJ.** 2011. Carnitine palmitoyltransferase-1c gain-of-function in the brain results in postnatal microencephaly. J. Neurochem. **118**:388–398.
15. **Pavlidis P, Ramaswami M, Tanouye MA.** 1994. The Drosophila easily shocked gene: a mutation in a phospholipid synthetic pathway causes seizure, neuronal failure, and paralysis. Cell **79**:23–33.
16. **Branstrom R, Corkey BE, Berggren PO, Larsson O.** 1997. Evidence for a unique long chain acyl-CoA ester binding site on the ATP-regulated potassium channel in mouse pancreatic beta cells. J. Biol. Chem. **272**: 17390–17394.
17. **Bränström R, Leibiger I, Leibiger B, Klement G, Nilsson J, Århem P, Aspinwall C, Corkey B, Larsson O, Berggren PO.** 2007. Single residue (K332A) substitution in Kir6.2 abolishes the stimulatory effect of long-chain acyl-CoA esters: indications for a long-chain acyl-CoA ester binding motif. Diabetologia **50**:1670–1677.
18. **Riedel MJ, Baczko I, Searle GJ, Webster N, Fercho M, Jones L, Lang J, Lytton J, Dyck JR, Light PE.** 2006. Metabolic regulation of sodium-calcium exchange by intracellular acyl CoAs. EMBO J. **25**:4605–4614.
19. **Shumilina E, Klocker N, Korniychuk G, Rapedius M, Lang F, Baukrowitz T.** 2006. Cytoplasmic accumulation of long-chain coenzyme A

esters activates KATP and inhibits Kir2.1 channels. J. Physiol. **575**:433–442.
20. **Tucker SJ, Baukrowitz T.** 2008. How highly charged anionic lipids bind and regulate ion channels. J. Gen. Physiol. **131**:431–438.
21. **Watkins PA.** 1997. Fatty acid activation. Prog. Lipid Res. **36**:55–83.
22. **Kirkby B, Roman N, Kobe B, Kellie S, Forwood JK.** 2010. Functional and structural properties of mammalian acyl-coenzyme A thioesterases. Prog. Lipid Res. **49**:366–377.
23. **Kang HW, Niepel MW, Han S, Kawano Y, Cohen DE.** 2012. Thioesterase superfamily member 2/acyl-CoA thioesterase 13 (Them2/Acot13) regulates hepatic lipid and glucose metabolism. FASEB J. **26**:2209–2221.
24. **Zhang Y, Li Y, Niepel MW, Kawano Y, Han S, Liu S, Marsili A, Larsen PR, Lee CH, Cohen DE.** 2012. Targeted deletion of thioesterase superfamily member 1 promotes energy expenditure and protects against obesity and insulin resistance. Proc. Natl. Acad. Sci. U. S. A. **109**:5417–5422.
25. **Hunt MC, Alexson SE.** 2002. The role Acyl-CoA thioesterases play in mediating intracellular lipid metabolism. Prog. Lipid Res. **41**:99–130.
26. **Yamada J, Kurata A, Hirata M, Taniguchi T, Takama H, Furihata T, Shiratori K, Iida N, Takagi-Sakuma M, Watanabe T, Kurosaki K, Endo T, Suga T.** 1999. Purification, molecular cloning, and genomic organization of human brain long-chain acyl-CoA hydrolase. J. Biochem. **126**:1013–1019.
27. **Guyenet SJ, Furrer SA, Damian VM, Baughan TD, La Spada AR, Garden GA.** 2010. A simple composite phenotype scoring system for evaluating mouse models of cerebellar ataxia. J. Vis Exp. **2010**:e1787. doi:10.3791/1787.
28. **Gao S, Kinzig KP, Aja S, Scott KA, Keung W, Kelly S, Strynadka K, Chohnan S, Smith WW, Tamashiro KLK, Ladenheim EE, Ronnett GV, Tu Y, Birnbaum MJ, Lopaschuk GD, Moran TH.** 2007. Leptin activates hypothalamic acetyl-CoA carboxylase to inhibit food intake. Proc. Natl. Acad. Sci. U. S. A. **104**:17358–17363.
29. **Eckel-Mahan KL, Patel VR, Mohney RP, Vignola KS, Baldi P, Sassone-Corsi P.** 2012. Coordination of the transcriptome and metabolome by the circadian clock. Proc. Natl. Acad. Sci. U. S. A. **109**:5541–5546.
30. **Folch J, Lees M, Sloane Stanley GH.** 1957. A simple method for the isolation and purification of total lipides from animal tissues. J. Biol. Chem. **226**:497–509.
31. **Ellis J, Li L, Wu P, Koves T, Ilkayeva O, Stevens R, Watkins S, Muoio D, Coleman R.** 2010. Adipose acyl-CoA synthetase-1 (ACSL1) directs fatty acids towards β-oxidation and is required for cold thermogenesis. Cell Metab. **12**:53–64.
32. **Bligh EG, Dyer WJ.** 1959. A rapid method of total lipid extraction and purification. Can. J. Biochem. Physiol. **37**:911–917.
33. **Yamada J.** 2005. Long-chain acyl-CoA hydrolase in the brain. Amino Acids **28**:273–278.
34. **Yamada J, Furihata T, Tamura H, Watanabe T, Suga T.** 1996. Long-chain acyl-CoA hydrolase from rat brain cytosol: purification, characterization, and immunohistochemical localization. Arch. Biochem. Biophys. **326**:106–114.
35. **Yamada J, Kuramochi Y, Takagi M, Suga T.** 2004. Expression of acyl-CoA hydrolase in the developing mouse brain. Neurosci. Lett. **355**:89–92.
36. **Lein ES, Hawrylycz MJ, Ao N, Ayres M, Bensinger A, Bernard A, Boe AF, Boguski MS, Brockway KS, Byrnes EJ, Chen L, Chen L, Chen TM, Chin MC, Chong J, Crook BE, Czaplinska A, Dang CN, Datta S, Dee NR, Desaki AL, Desta T, Diep E, Dolbeare TA, Donelan MJ, Dong HW, Dougherty JG, Duncan BJ, Ebbert AJ, Eichele G, Estin LK, Faber C, Facer BA, Fields R, Fischer SR, Fliss TP, Frensley C, Gates SN, Glattfelder KJ, Halverson KR, Hart MR, Hohmann JG, Howell MP, Jeung DP, Johnson RA, Karr PT, Kawal R, Kidney JM, Knapik RH, Kuan CL, et al.** 2007. Genome-wide atlas of gene expression in the adult mouse brain. Nature **445**:168–176.
37. **Hunt MC, Greene S, Hultenby K, Svensson LT, Engberg S, Alexson SE.** 2007. Alternative exon usage selectively determines both tissue distribution and subcellular localization of the acyl-CoA thioesterase 7 gene products. Cell. Mol. Life Sci. **64**:1558–1570.
38. **Xu Y, Nedungadi TP, Zhu L, Sobhani N, Irani BG, Davis KE, Zhang X, Zou F, Gent LM, Hahner LD, Khan SA, Elias CF, Elmquist JK, Clegg DJ.** 2011. Distinct hypothalamic neurons mediate estrogenic effects on energy homeostasis and reproduction. Cell Metab. **14**:453–465.
39. **Gao Q, Wolfgang MJ, Neschen S, Morino K, Horvath TL, Shulman GI, Fu XY.** 2004. Disruption of neural signal transducer and activator of transcription 3 causes obesity, diabetes, infertility, and thermal dysregulation. Proc. Natl. Acad. Sci. U. S. A. **101**:4661–4666.
40. **Forwood JK, Thakur AS, Guncar G, Marfori M, Mouradov D, Meng W, Robinson J, Huber T, Kellie S, Martin JL, Hume DA, Kobe B.** 2007. Structural basis for recruitment of tandem hotdog domains in acyl-CoA thioesterase 7 and its role in inflammation. Proc. Natl. Acad. Sci. U. S. A. **104**:10382–10387.
41. **Broustas CG, Hajra AK.** 1995. Purification, properties, and specificity of rat brain cytosolic fatty acyl coenzyme A hydrolase. J. Neurochem. **64**:2345–2353.
42. **Carper MJ, Zhang S, Turk J, Ramanadham S.** 2008. Skeletal muscle group VIA phospholipase A2 (iPLA2β): expression and role in fatty acid oxidation. Biochemistry **47**:12241–12249.
43. **Zhuravleva E, Gut H, Hynx D, Marcellin D, Bleck CK, Genoud C, Cron P, Keusch JJ, Dummler B, Esposti MD, Hemmings BA.** 2012. Acyl coenzyme A thioesterase Them5/Acot15 is involved in cardiolipin remodeling and fatty liver development. Mol. Cell. Biol. **32**:2685–2697.
44. **Etschmaier K, Becker T, Eichmann TO, Schweinzer C, Scholler M, Tam-Amersdorfer C, Poeckl M, Schuligoi R, Kober A, Chirackal Manavalan AP, Rechberger GN, Streith IE, Zechner R, Zimmermann R, Panzenboeck U.** 2011. Adipose triglyceride lipase affects triacylglycerol metabolism at brain barriers. J. Neurochem. **119**:1016–1028.
45. **Obici S, Feng Z, Arduini A, Conti R, Rossetti L.** 2003. Inhibition of hypothalamic carnitine palmitoyltransferase-1 decreases food intake and glucose production. Nat. Med. **9**:756–761.
46. **Obici S, Feng Z, Morgan K, Stein D, Karkanias G, Rossetti L.** 2002. Central administration of oleic acid inhibits glucose production and food intake. Diabetes **51**:271–275.
47. **Wang R, Cruciani-Guglielmacci C, Migrenne S, Magnan C, Cotero VE, Routh VH.** 2006. Effects of oleic acid on distinct populations of neurons in the hypothalamic arcuate nucleus are dependent on extracellular glucose levels. J. Neurophysiol. **95**:1491–1498.
48. **Le Foll C, Irani BG, Magnan C, Dunn-Meynell AA, Levin BE.** 2009. Characteristics and mechanisms of hypothalamic neuronal fatty acid sensing. Am. J. Physiol. Regul. Integr. Comp. Physiol. **297**:R655–R664.
49. **Bouteloup C, Desport JC, Clavelou P, Guy N, Derumeaux-Burel H, Ferrier A, Couratier P.** 2009. Hypermetabolism in ALS patients: an early and persistent phenomenon. J. Neurol. **256**:1236–1242.
50. **Dupuis L, Pradat PF, Ludolph AC, Loeffler JP.** 2011. Energy metabolism in amyotrophic lateral sclerosis. Lancet Neurol. **10**:75–82.
51. **Israelson A, Arbel N, Da Cruz S, Ilieva H, Yamanaka K, Shoshan-Barmatz V, Cleveland DW.** 2010. Misfolded mutant SOD1 directly inhibits VDAC1 conductance in a mouse model of inherited ALS. Neuron **67**:575–587.
52. **Ghosh T, Pandey N, Maitra A, Brahmachari SK, Pillai B.** 2007. A role for voltage-dependent anion channel Vdac1 in polyglutamine-mediated neuronal cell death. PLoS One **2**:e1170. doi:10.1371/journal.pone.0001170.
53. **Yamada J, Furihata T, Iida N, Watanabe T, Hosokawa M, Satoh T, Someya A, Nagaoka I, Suga T.** 1997. Molecular cloning and expression of cDNAs encoding rat brain and liver cytosolic long-chain acyl-CoA hydrolases. Biochem. Biophys. Res. Commun. **232**:198–203.
54. **Kuramochi Y, Takagi-Sakuma M, Kitahara M, Emori R, Asaba Y, Sakaguchi R, Watanabe T, Kuroda J, Hiratsuka K, Nagae Y, Suga T, Yamada J.** 2002. Characterization of mouse homolog of brain acyl-CoA hydrolase: molecular cloning and neuronal localization. Mol. Brain Res. **98**:81–92.
55. **Ter Beek A, Keijser BJ, Boorsma A, Zakrzewska A, Orij R, Smits GJ, Brul S.** 2008. Transcriptome analysis of sorbic acid-stressed Bacillus subtilis reveals a nutrient limitation response and indicates plasma membrane remodeling. J. Bacteriol. **190**:1751–1761.
56. **Dongol B, Shah Y, Kim I, Gonzalez FJ, Hunt MC.** 2007. The acyl-CoA thioesterase I is regulated by PPARalpha and HNF4alpha via a distal response element in the promoter. J. Lipid Res. **48**:1781–1791.
57. **Durgan DJ, Smith JK, Hotze MA, Egbejimi O, Cuthbert KD, Zaha VG, Dyck JR, Abel ED, Young ME.** 2006. Distinct transcriptional regulation of long-chain acyl-CoA synthetase isoforms and cytosolic thioesterase 1 in the rodent heart by fatty acids and insulin. Am. J. Physiol. Heart Circ. Physiol. **290**:H2480–H2497.
58. **Yamada J, Kuramochi Y, Takoda Y, Takagi M, Suga T.** 2003. Hepatic induction of mitochondrial and cytosolic acyl-coenzyme A hydrolases/thioesterases in rats under conditions of diabetes and fasting. Metab. Clin. Exp. **52**:1527–1529.
59. **Yang JW, Czech T, Yamada J, Csaszar E, Baumgartner C, Slavc I, Lubec G.** 2004. Aberrant cytosolic acyl-CoA thioester hydrolase in hippocampus of patients with mesial temporal lobe epilepsy. Amino Acids **27**:269–275.

60. **Lin Y, Bloodgood BL, Hauser JL, Lapan AD, Koon AC, Kim TK, Hu LS, Malik AN, Greenberg ME.** 2008. Activity-dependent regulation of inhibitory synapse development by Npas4. Nature **455**:1198–1204.
61. **Bough KJ, Wetherington J, Hassel B, Pare JF, Gawryluk JW, Greene JG, Shaw R, Smith Y, Geiger JD, Dingledine RJ.** 2006. Mitochondrial biogenesis in the anticonvulsant mechanism of the ketogenic diet. Ann. Neurol. **60**:223–235.
62. **Cahill GF, Jr.** 2006. Fuel metabolism in starvation. Annu. Rev. Nutr. **26**:1–22.
63. **Hakak Y, Walker JR, Li C, Wong WH, Davis KL, Buxbaum JD, Haroutunian V, Fienberg AA.** 2001. Genome-wide expression analysis reveals dysregulation of myelination-related genes in chronic schizophrenia. Proc. Natl. Acad. Sci. U. S. A. **98**:4746–4751.
64. **Wishart TM, Paterson JM, Short DM, Meredith S, Robertson KA, Sutherland C, Cousin MA, Dutia MB, Gillingwater TH.** 2007. Differential proteomics analysis of synaptic proteins identifies potential cellular targets and protein mediators of synaptic neuroprotection conferred by the slow Wallerian degeneration (Wlds) gene. Mol. Cell. Proteomics **6**:1318–1330.